POLARIZED DEEP INELASTIC SCATTERING: DATA ANALYSIS AND RESULTS**

BARBARA BADEŁEK

Institute of Physics, University of Uppsala, S-751 21 Uppsala, Sweden
and
Institute of Experimental Physics, Warsaw University,
Hoża 69, PL-00 681 Warsaw, Poland

(Received January 14, 1997)

Spin properties of the nucleon are discussed based on the ongoing and planned measurements. Rôle, method and features of radiative corrections applied in the analyses are presented. Future prospects of the spin physics are reviewed.

PACS numbers: 14.20. Dh

1. Introduction

Interest in spin phenomena in deep inelastic scattering revived in the eighties after the European Muon Collaboration, EMC, discovered [1] that the quark contribution to the proton spin is substantially smaller than expected. The problem of origin of the proton spin has then led to an intense experimental and theoretical activity. Experiments of new generation were set up, in which a (deep) inelastic scattering of polarized charged leptons off polarized proton and deuteron target was precisely studied. The experiments delivered very accurate and compatible data, confirming the original result of the EMC and permitting precise QCD analyses and tests of fundamental sum rules. The region of low x turned out to be of particular interest, in analogy to the unpolarized deep inelastic scattering.

In spite of all this progress and effort, the main question, that about the origin of the proton spin has not yet been answered conclusively. Old questions have been replaced by new ones and new goals are being set. In this article we review the experimental results on spin structure functions

* Presented at the Cracow International Symposium on Radiative Corrections to the Standard Model, Cracow, Poland, August 1–5, 1996.

** This research has been supported in part by the Polish State Committee for Scientific Research grant number 2P03B 184 10.

and derived quantities and their interpretations. In accordance with the topic of this conference we discuss in more detail a method of applying the radiative corrections in the data analysis.

2. Formalism

The deep inelastic lepton–nucleon scattering cross section is a sum of a spin independent term $\overline{\sigma}$ and a term proportional to the lepton helicity, $h_l = \pm 1$:

$$\sigma = \overline{\sigma} - \tfrac{1}{2} h_l \Delta\sigma. \tag{1}$$

(symbols denote double differential cross sections). In the one photon–exchange approximation, the differential electroproduction spin-averaged cross section, $\overline{\sigma}$, is related to the structure function $F_2(x, Q^2)$ and the ratio $R(x, Q^2)$ of the cross sections for the longitudinally and transversally polarized virtual photons by

$$\frac{d^2\overline{\sigma}(x, Q^2)}{dQ^2 dx} = \\ = \frac{4\pi\alpha^2}{Q^4 x}\left\{1 - y - \frac{Mxy}{2E} + \left(1 - \frac{2m^2}{Q^2}\right)\frac{y^2(1 + 4M^2x^2/Q^2)}{2[1 + R(x, Q^2)]}\right\} F_2(x, Q^2), \tag{2}$$

where M and m are masses of the proton and electron (muon) respectively, E and ν are the incident lepton energy and the energy transfer in the target rest frame, $y = \nu/E$, $x = Q^2/(2M\nu)$ and α is the electromagnetic coupling constant. Information on the function $R(x, Q^2)$, which has so far been measured only in fixed-target experiments, is scarce. On the contrary, $F_2(x, Q^2)$ is known precisely in a wide kinematic range, see *e.g.* [2].

In the spin dependent part of Eq. (1), only longitudinally polarized leptons will be considered. Cross section $\Delta\sigma$ gives only a small contribution to the total deep inelastic cross section and in the one photon–exchange approximation it depends on the two structure functions $g_1(x, Q^2)$ and $g_2(x, Q^2)$ as follows:

$$\Delta\sigma = \cos\psi\, \Delta\sigma_{\parallel} + \sin\psi\, \cos\phi\, \Delta\sigma_{\perp}, \tag{3}$$

where

$$\frac{d^2\Delta\sigma_{\parallel}}{dx\, dQ^2} = \frac{16\pi\alpha^2 y}{Q^4}\left[(1 - \frac{y}{2} - \frac{\gamma^2 y^2}{4}) g_1(x, Q^2) - \frac{\gamma^2 y}{2} g_2(x, Q^2)\right], \\ \frac{d^3\Delta\sigma_T}{dx\, dQ^2\, d\phi} = -\cos\phi\, \frac{8\alpha^2 y}{Q^4}\gamma\sqrt{1 - y - \frac{\gamma^2 y^2}{4}}\left[\frac{y}{2} g_1(x, Q^2) + g_2(x, Q^2)\right]. \tag{4}$$

In the above, ψ denotes the angle between the lepton and the nucleon spin and ϕ the angle between the scattering plane and the spin plane; furthermore $\Delta\sigma_\perp = \Delta\sigma_T/\cos\phi$ and $\gamma = 2Mx/\sqrt{Q^2}$ is a kinematical factor, small within the acceptance of high energy experiments.

The following two cross section asymmetries are usually measured in the experiments:

$$A_{\parallel} = \frac{\Delta\sigma_{\parallel}}{2\overline{\sigma}} \qquad \text{and} \qquad A_{\perp} = \frac{\Delta\sigma_{\perp}}{2\overline{\sigma}}. \tag{5}$$

These asymmetries are expressed in terms of asymmetries A_1 and A_2, often interpreted as virtual photon–nucleon asymmetries:

$$A_{\parallel} = D(A_1 + \eta A_2), \qquad A_{\perp} = d(A_2 - \xi A_1), \tag{6}$$

where

$$A_1 = \frac{g_1 - \gamma^2 g_2}{F_1}, \qquad A_2 = \gamma\frac{g_1 + g_2}{F_1}. \tag{7}$$

D and d, often called the depolarization factors of the virtual photon, depend on y and on R; factors η and ξ depend only on kinematic variables and are small in the kinematic regions covered by the present experiments. The bounds $|A_1| \leq 1$, $|A_2| \leq \sqrt{R}$ are satisfied.

From the above formulae:

$$g_1 \approx A_1 F_1 \approx \frac{A_{\parallel}}{D}\frac{F_2}{2x(1+R)}. \tag{8}$$

Within the QPM, the spin dependent structure function g_1 is given by

$$g_1(x) = \frac{1}{2}\sum_{i=1}^{n_f} e_i^2[\Delta q_i(x) + \Delta\bar{q}_i(x)], \tag{9}$$

with $\Delta q_i(x) = q_i^+(x) - q_i^-(x)$, where $q^{\pm}$ are the distribution functions of quarks with spin parallel (antiparallel) to the nucleon spin. Less obvious is the meaning of g_2 which contains a leading twist part, completely determined by g_1 and a higher twist part, the meaning of which is subject to debate [3].

In QCD, g_1 evolves according to Altarelli–Parisi equations, similar to the unpolarized ones. Corresponding coefficient and splitting functions have recently been calculated in the $\overline{MS}$ renormalisation scheme, up to order α_S^2 [4], permitting the next-to-leading order QCD analysis of g_1 and thus a determination of the polarized parton distributions, $\Delta q_i(x, Q^2)$. The valence quark distributions $\Delta u_v(x, Q^2)$ and $\Delta d_v(x, Q^2)$ can be determined with some accuracy from the data, while the polarized sea quark and gluon distributions $\Delta\bar{q}(x, Q^2)$ and $\Delta g(x, Q^2)$ are only loosely constrained by the structure function measurements, see *e.g.* [5] for the comparison of the leading order distributions.

Contrary to g_1 and g_2, definite theoretical predictions exist for the first moment of g_1, $\Gamma_1 = \int_0^1 g_1(x)\,dx$: the Bjorken and the Ellis–Jaffe sum rules.

3. Sum rules

Several sum rules have been formulated for different combinations of structure functions. Strict QCD predictions, valid for $Q^2 \to \infty$, exist for those involving only flavour nonsinglet contributions, *e.g.* the Bjorken sum rule. Experimental measurements of such sum rules provide a stringent test of fundamental QCD assumptions. They also in principle permit the extraction of the strong coupling constant, α_S, from the data. Due to the finite Q^2 of the measurements, a predicted value of a sum rule is usually presented in the form of a power series in α_S, the coefficients of which are directly calculated.

There is no strict QCD prediction for the sum rules containing the flavour singlet contributions, *e.g.* the Ellis–Jaffe sum rules. The reason is that singlet contributions contain an 'intrinsic' Q^2 dependence due to the anomalous dimension of the singlet axial vector current. Testing them usually results in surprises which teach us a lot about the shortcomings of the simple quark model.

In the experimental tests of the sum rules, a major source of systematic errors is a limited experimental acceptance in Q^2 at each x value. This usually means that a sum rule is measured at a certain Q_0^2, common to all points but at values of Q_0^2 which are not sufficiently high to exclude a contribution from nonperturbative effects ('higher twists'). Higher twist effects in the Q^2 dependence of Γ_1 will not be considered here. They are likely to be negligible, at least at $Q^2 > 1$ GeV^2.

All the sum rules involve integrations of observables over the whole $0 \leq x \leq 1$ interval. This means that due to the limited experimental acceptance, extrapolations from $x_{\min}$ to 0 and from $x_{\max}$ to 1 have to be performed. These extrapolations are another source of systematic uncertainties in the sum rules' tests. In particular, evaluation of Γ_1 requires extrapolations of g_1 to x equal 0 and 1. The latter is not critical since $g_1 \to 0$ at $x \to 1$ but the former is a considerable problem since g_1 is probably not constant as x decreases and thus its contribution to Γ_1 at low x may be sizable.

3.1. Low x behaviour of g_1

The data suggest a difference in the small x behaviour of g_1^p and g_1^n (*c.f.* Section 5) and that indicates a sizable non-singlet contribution to g_1 in that region. Expectations concerning the g_1 behaviour at small x, based on the QCD calculations are twofold: (1) resummation of standard Altarelli–Parisi corrections gives, [6, 7]: $g_1(x) \sim \exp\left[A\sqrt{\ln(\alpha_s(Q_0^2)/\alpha_s(Q^2))\ln(1/x)}\right]$ for nonsinglet and singlet part of g_1; (2) resummation of leading powers of $\ln(1/x)$ gives: $g_1^{ns}(x) \sim 1/x^{\omega_{ns}}$, $\omega_{ns} \simeq 0.4$, [8] and $g_1^s(x) \sim 1/x^{\omega_s}$,

$\omega_s \simeq 3\omega_{ns} > 1$, [9] where indices '$s$' and '$ns$' refer to singlet- and non-singlet contributions to g_1. Inconsistent with the above is the Regge prediction, that $g_1^p + g_1^n$ and $g_1^p - g_1^n$ behave like $x^{-\alpha}$, [10]. The lowest contributing Regge trajectories are those of the pseudovector mesons f_1 (for the isosinglet combination, $g_1^p + g_1^n$) and a_1 (for the isotriplet combination, $g_1^p - g_1^n$). Their intercepts are negative and assumed to be equal: $-0.5 < \alpha < 0$. Finally a flavour singlet contribution to $g_1(x)$ that varies as (2ln(1/x)-1) was obtained from a model where an exchange of two nonperturbative gluons is assumed, [11]. Even very divergent forms like $g_1(x) \sim (x \ln^2 x)^{-1}$ have been considered, [12].

Results on Γ_1 thus depend on the assumptions made in the $x \to 0$ extrapolation. Both SMC and SLAC experiments assume the Regge like behaviour of g_1, $g_1 \sim x^{-\alpha}$, with α=0. A value of g_1 is evaluated as an average at the two lowest x data points and a resulting contribution from the unmeasured region in (low) x to the Γ_1 is estimated. This contribution is then taken as a measure of the corresponding contribution to the systematic error on Γ_1.

3.2. The flavour nonsinglet (Bjorken) sum rule

This sum rule was obtained by Bjorken [13] from the current algebra and isospin symmetry between the proton and the neutron:

$$\Gamma_1^p - \Gamma_1^n = \frac{1}{6}\left|\frac{g_A}{g_V}\right| = \frac{1}{6}(\Delta u - \Delta d)\,, \tag{10}$$

where g_A and g_V are the axial and vector weak coupling constants in the neutron beta decay and Δq denote first moments of the spin dependent parton distributions in the proton, $\Delta q = \int_0^1 \Delta q_i(x)dx$. This sum rule has later been derived in the QCD and is one of the strict predictions made by this theory. The QCD corrections to (10) have been computed up to the order α_S^3 [14] and the $\mathcal{O}(\alpha_S^4)$ have been estimated [15].

3.3. The flavour singlet (Ellis-Jaffe) sum rules

Separate sum rules, obtained by Ellis and Jaffe [16], hold for the proton and the neutron:

$$\Gamma_1^{p(n)} = \pm\frac{1}{12}\left|\frac{g_A}{g_V}\right| + \frac{1}{36}a_8 + \frac{1}{9}\Delta\Sigma\,. \tag{11}$$

Here $\Delta\Sigma = \Delta u + \Delta d + \Delta s$ is the flavour singlet axial coupling, $a_8 = 3F - D$ and $|g_A/g_V| = F + D$ are related to the symmetric and antisymmetric weak flavour-SU(3) couplings (F and D) in the baryon octet and Δq were defined in Sec. 3.2. If the flavour-SU(3) is exact then a_8 can be predicted from

measurements of hyperon decays. There is however no prediction for $\Delta\Sigma$, except when Δs=0. In this case $\Delta\Sigma = a_8 \sim 0.6$, as was assumed in the original formulation by Ellis and Jaffe [16]. QCD corrections to these sum rules have been calculated up to the order α_S^2 [17] and the $\mathcal{O}(\alpha_S^3)$ have been estimated [18]. Due to the axial anomaly of the singlet axial vector current, $\Delta\Sigma$ is intrinsically Q^2–dependent. Depending on the factorization scheme applied [19] this results either in a scale–dependence of the sea quark polarization or in an extra contribution to the Ellis–Jaffe sum rule, involving $\Delta g = \int_0^1 [g^+(x) - g^-(x)]\, dx$, the gluonic equivalent of the quark distribution moments. Both formulations are equivalent.

4. Experiments and elements of data analysis

Until recently the experimental knowledge on the spin structure functions came entirely from conventional fixed-target setups: EMC and Spin Muon Collaboration, SMC, at CERN and experiments at SLAC. Now it is being complemented by the results from the unconventional though *par excellance* fixed-target, HERMES experiment, at the HERA $e-p$ collider. Experiments with polarized beams at colliders are also planned.

The fixed-target electron (muon) scattering experiments are inclusive, *i.e.* information on the kinematic variables comes only from measurements of the incident and scattered leptons. Hadrons resulting from the target breakup are also measured, however their identification until now was incomplete.

New generation polarized deep inelastic scattering (DIS) experiments are listed in Table I and their kinematic coverage is shown in Fig. 1.

TABLE I

New generation experiments on polarized deep inelastic charged lepton–nucleon scattering. The last column shows references to the principal physics results obtained until now, (from [20], updated).

Experiment	Beam	Year	Beam energy (GeV)	Target	References
SMC	μ^+	1992–5	100,190	C_4D_9OD	[21, 22, 23]
		1993	190	C_4H_9OH	[24, 25, 26]
		1996	190	NH_3	
E142	e^-	1992	19.4 –25.5	^3He	[27, 28]
E143	e^-	1993	29.1	NH_3, ND_3	[29, 30, 31]
E154	e^-	1995	50	^3He	[32]
E155	e^-	1996	50	NH_3, ND_3	
HERMES	e^-	1995–	30–35	H, D, ^3He	[33]

In DIS experiments the low x region is correlated with low values of Q^2 and the range of Q^2 covered at low x is very limited. The lowest values of x were reached by the SMC at CERN by applying special experimental techniques permitting measurements of muon scattering angles as low as 1 mrad. These 'small x triggers' and special off-line selection methods were also effective against the background of muons scattered elastically from target atomic electrons which produce a peak at x =0.000545.

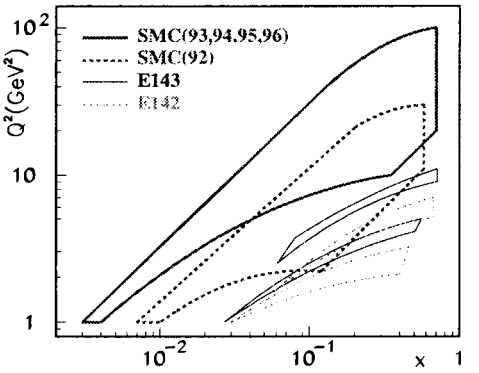

Fig. 1. Kinematic range of measurements by certain polarized DIS experiments. Two areas for SMC refer to runs with 100 (1992) and 190 (1993–1996) GeV incident muon energy. For each of the two SLAC experiments, E142 and E143, two areas correspond to two spectrometer arms. The SMC has recently extended their analysis to $x \sim 10^{-5}$ and Q^2 values substantially lower than 1 GeV^2. Acceptance of HERMES slightly extends that of SLAC experiments. Figure taken from [34].

Charged lepton DIS experiments benefit from high rates and low (unfortunately complicated) systematic biases. They however have to deal with a strong Q^2 dependence of the cross section (photon propagator effects) and with large contribution of radiative processes. Electron and muon measurements are complementary: the former offers very high beam intensities and thus statistics but its kinematic acceptance is limited to low values of Q^2 and moderate values of x, the latter extends to higher Q^2 and down to low values of x (an important aspect in the study of sum rules) but due to limited muon intensities the data taking time has to be long to ensure a satisfactory statistics.

The SMC experiment at CERN uses a naturally polarized muon beam (~80 % polarization) and a double-cell, cryogenic, solid state target. The beam polarization at the SMC has been measured with a purpose-built polarimeter, using two independent methods: polarized μe scattering and an analysis of the energy spectrum of electrons coming from the muon decay.

Average polarization of the target was about 86% and 50% for the butanol (proton) and deuterated butanol (deuteron) respectively. Experiments E142 – E155 at SLAC use an electron beam (polarization about 86%; E142 - 40%) and liquid (solid) cryogenic targets (polarization reached 80% for the proton and 25% for the deuteron one in E143; for the ^{3}He gas target: ~30%). The HERMES experiment at DESY uses a self-polarized (in ~50%) electron beam from the HERA collider and internal gas targets (polarization ~50% for ^{3}He). Frequent exchange of target- (SMC, HERMES) and beam (SLAC) polarizations permitted to greatly reduce systematic errors on cross section asymmetries. The scattered muon spectrometers in the SMC and SLAC experiments have been used (with little change) in DIS experiments proceeding the polarized programme, contrary to the HERMES, purpose-built apparatus.

The cross section asymmetry measured in the polarized lepton–polarized nucleon experiments, $A_{\rm exp}$, is related to the asymmetries defined in Eq. (5) by

$$A_{\rm exp} = f P_{\rm t} P_{\rm b} A\,, \tag{12}$$

where $P_{\rm t}, P_b$ denote the target and beam polarizations and f, the target dilution factor, accounts for the fact that only a fraction of nucleons is polarized. Dilution factors are about 0.10-0.2 in the SMC and SLAC and 1 at HERMES proton target (0.3 for the ^{3}He target).

4.1. Radiative corrections in the data analysis

The structure functions, polarized as well as unpolarized were defined for the one-photon exchange reaction, *c.f.* equations (2),(4). Higher order QED corrections, which we have ignored so far, have thus to be applied to the measured asymmetries, (12), to convert them to the single-photon asymmetries. These 'radiative corrections' have to be applied in two places: in the evaluation of the dilution factor and in the asymmetry, [35]. Below we give a short account of the method used by the SMC; methods used by HERMES and SLAC are similar.

Understanding of the radiative corrections procedure will be facilitated by introducing in this section an extended notation. The measured observables will acquire superscripts 't' ('total', *i.e.* comprising all radiative processes) and one-gamma exchange functions – superscripts '1γ'. In this way, a cross section measured in a polarized experiment is related in the following way to the one-gamma cross section: $\sigma^{\rm t} = v\sigma^{1\gamma} + \sigma_{\rm tail}$. Analogous relation holds for spin-independent cross section: $\overline{\sigma}^{\rm t} = v\overline{\sigma}^{1\gamma} + \overline{\sigma}_{\rm tail}$. Here v which mostly accounts for vacuum polarization, was found to be close to unity and thus subsequently put equal to 1; $\sigma_{\rm tail}$ ($\overline{\sigma}_{\rm tail}$) are contributions from the elastic, quasi-elastic and inelastic lepton–nucleon and lepton–nucleus scat-

tering. A direct consequence of the above equations is the following relation between a measured- and one-photon exchange asymmetries:

$$A_1^{\mathrm{t}} = \rho[A_1^{1\gamma} + (\delta A_1)^{\mathrm{rc}}]. \tag{13}$$

The factor $\rho = v\overline{\sigma}^{1\gamma}/\overline{\sigma}^{\mathrm{t}}$ in the above equation was evaluated using the program TERAD [36] and its value differed from unity at most by 2%. The additive term $(\delta A_1)^{\mathrm{rc}} = (\delta A_{\|}/D)^{\mathrm{rc}} = (\Delta\sigma)_{\mathrm{tail}}/2Dv\overline{\sigma}^{1\gamma}$, was evaluated using the program POLRAD [37, 38]. The factor ρ has been incorporated in the evaluation of the dilution factor, see below. Magnitude of the additive correction $(\delta A_1)^{\mathrm{rc}}$ is displayed in Fig. 2.

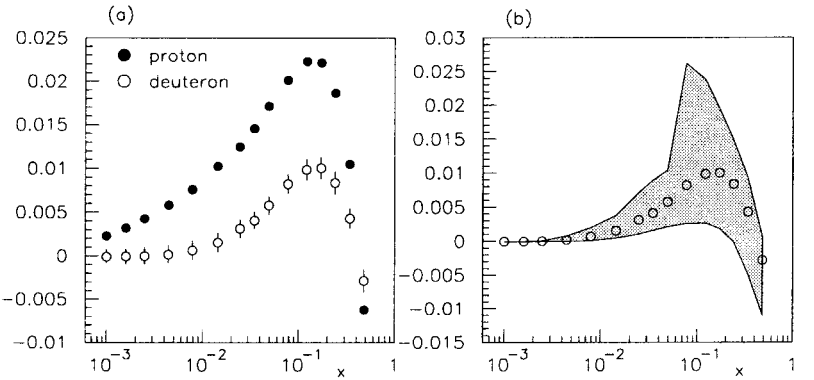

Fig. 2. (a) Radiative correction term $(\delta A_1)^{\mathrm{rc}}$ for the proton and deuteron target as a function of x. (b) Same term for the proton target. A band around points shows a variation of the correction in each bin, due to its changes with Q^2 (or y). Figure taken from [34].

The additive correction was evaluated for both $A_{\|}^{\mathrm{t}}$ and $A_{\perp}^{\mathrm{t}}$. The asymmetry $A_1^{\mathrm{p}}(x)$ required for these calculations in POLRAD is taken from Refs. [1, 25, 29]. In the longitudinal case the contribution from A_2^{p} is neglected. The uncertainty of $(\delta A_1)^{\mathrm{rc}}$ is estimated by varying the input values of A_1^{p} within the errors. The radiative corrections to the transverse asymmetry $A_{\perp}^{\mathrm{t}}$ were evaluated assuming that $g_2 = g_2^{\mathrm{WW}}$ [39]. The corrections are much smaller than the statistical error of $A_{\perp}$ and therefore the additive correction has been neglected.

In addition to butanol (or deuterated butanol), the target cells contain other chemical elements. Thus the dilution factor f can be expressed in terms of the number n_A of nuclei with mass number A and the corresponding spin-averaged cross sections $\overline{\sigma}_A$ per nucleon, which include higher order QED

effects, for all the elements involved:

$$f = \frac{n_{\mathrm{H}} \cdot \overline{\sigma}^{\mathrm{t}}_{\mathrm{H}}}{\sum_A n_A \cdot \overline{\sigma}^{\mathrm{t}}_A}. \tag{14}$$

The one-photon exchange cross-section ratios $\overline{\sigma}^{1\gamma}_A/\overline{\sigma}^{1\gamma}_{\mathrm{H}}$ for D, He, C and Ca required for the calculation of f are obtained from the structure function ratios F_2^d/F_2^{p} [40] and F_2^A/F_2^d [41]. The cross section ratios $\overline{\sigma}^{1\gamma}_A/\overline{\sigma}^{1\gamma}_{\mathrm{H}}$ are converted to $\overline{\sigma}^{\mathrm{t}}_A/\overline{\sigma}^{\mathrm{t}}_H$ using TERAD. For unmeasured nuclei the cross section ratios are obtained in the same way from a parameterization of $F_2^A(x)/F_2^d(x)$ as a function of A, [42].

For the actual evaluation of asymmetries (5) employing (12) we use an effective dilution factor f'

$$f' = \rho f, \tag{15}$$

which accounts for the multiplicative part of the radiative correction to the asymmetry by including ρ as part of an event weight.

The dilution factors f and f' for the proton target are shown as a solid and broken lines in Fig. 3 and are compared to the 'naive' expectation for a mixture of 62% butanol, ($CH_3(CH_2)_3OH$), and 38% helium by volume, *i.e.*, $f \simeq 0.123$. The rise of f at $x > 0.3$ is due to the strong decrease with x of the ratio F_2^d/F_2^{p}, whereas the drop in the low x-range is due to the dilution by radiative events.

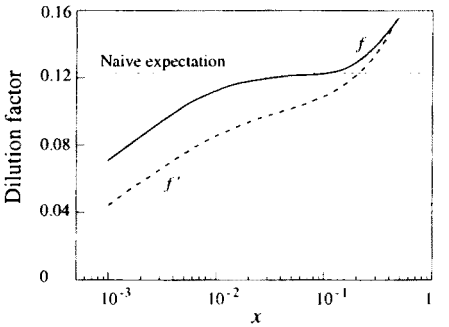

Fig. 3. The dilution factor f as a function of x for the SMC proton target (solid line). The dashed line shows an effective dilution factor, f'. The horizontal dashed line shows the naive expectation. Figure taken from [24].

Radiative events populate heavily the lowest x bins of the observables in the SMC kinematic range. These events are corrected for only on the level of the asymmetry determination. However they constitute a background and thus should be removed from the sample before the statistical accuracy

of measurements is determined. The way the SMC applied radiative corrections in their previous analyses resulted in retaining these events for the statistical error determination and, as a consequence, in the underestimation of statistical errors on asymmetries, especially at low x. The new procedure, described above, guarantees a proper calculation of the statistical error in the asymmetry, in contrast to the previous SMC analyses [25, 26, 21, 22] where the formula $A_1^{\rm t} = A_1^{1\gamma} + (\delta A_1)^{\rm rc}_{\rm old}$ was used instead of Eq. (13). The new procedure resulted in an increase in the A_1 statistical error by a factor of $1/\rho$ which reaches 1.4 at smallest x. It will be introduced in the forthcoming SMC publications, [24, 23]. It should be mentioned that measured values of the asymmetries remain (practically) unaffected by the change in the method. Details of the old and new procedures are given in [35].

5. Results of the measurements and spin structure of the nucleon

5.1. Results for asymmetries, spin structure functions and their moments

Cross section asymmetries A_1 and spin dependent structure functions g_1 have been measured for the proton and deuteron targets by the SMC, [21, 22, 25, 24, 26, 23] and by the E143, [29, 30].

Information on the neutron has been evaluated from the data on ^{3}He (E142, [27, 28], E154, [32], HERMES, [33]) and from the data on the proton and deuteron (SMC, 21–23). All data sets are in a very good mutual agreement even if A_1, extracted from data covering different Q^2 intervals, has been assumed to be Q^2 independent.

Results on A_1^p from different experiments are shown in Fig. 4. The average Q^2 of SMC and SLAC data is different by a factor of 7 thus suggesting that within the present accuracy, no Q^2 dependence of A_1^p is observed in the data – a conclusion holding also for A_1^d, [23] and in both cases confirmed by direct studies. The SMC measurements at $Q^2 < 1$ GeV^2, shown in Fig. 4, were not used in the analysis of g_1^p and evaluation of moments.

Results on A_2^p are shown in Fig. 5, [24]; together with the results for A_2^d, [23], they show that this function is significantly smaller than the bound $\sqrt{R}$ and consistent with zero.

Conversion of A_1 to g_1, which was made under an assumption that A_1 scales, needs information on the structure function F_1 or, equivalently, F_2 and R and about A_2 (*c.f.* Eq. (7)). The NMC parameterization of $F_2(x, Q^2)$ [43] and the SLAC parameterization of $R(x, Q^2)$ [44] have been used by both SMC and SLAC. However g_1 at average Q^2 is nearly (*i.e.* apart from radiative corrections) independent of R if the same R is used in extraction of F_2 and g_1. In the SMC data analysis A_2 was neglected; SLAC also assumed A_2=0, except in the E143 proton analysis, [29] where the measured A_2 was employed.

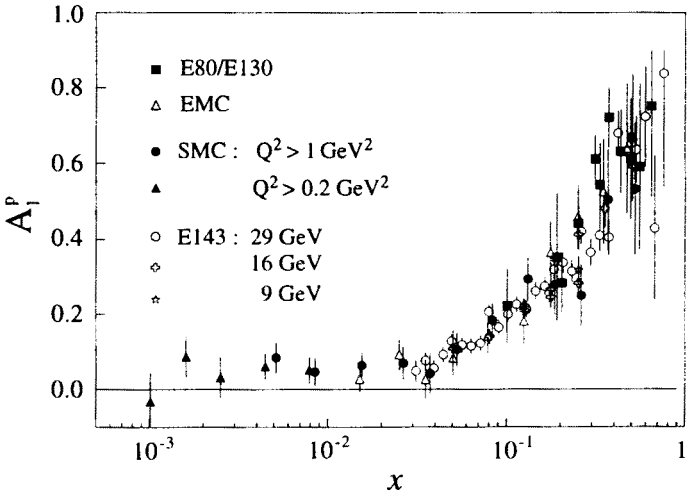

Fig. 4. The virtual photon asymmetry A_1^p as a function of x from SMC, EMC, SLAC E80, E130 and E143. Error bars are statistical. Figure taken from [24].

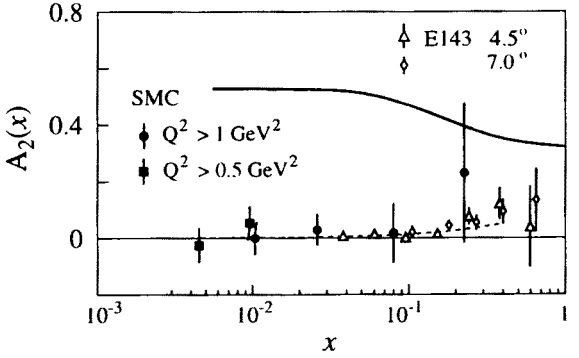

Fig. 5. Results for the $A_2^p(x)$ at Q^2 =5 GeV^2. The solid line shows the limit $|A_2| < \sqrt{R}$. Data from E143 are extrapolated to the same Q^2 assuming that $\sqrt{Q^2}A_2$ scales. Figure taken from [24].

Results on g_1 for proton, deuteron and neutron g_1 for the SMC measurements are shown in Fig. 6, [45]. Here $g_1^n = 2g_1^d/(1-1.5\omega_D) - g_1^p$ where $\omega_D \sim 0.05$ is the probability of the D-state of the deuteron. A very precise, though kinematically limited (x >0.015) measurement of g_1^n has been presented by the SLAC E154 Collaboration, [32]. The behaviour of the g_1^p seems to be different from that of g_1^d and g_1^n, especially at low x. This should be contrasted with the unpolarized case where a small difference between proton

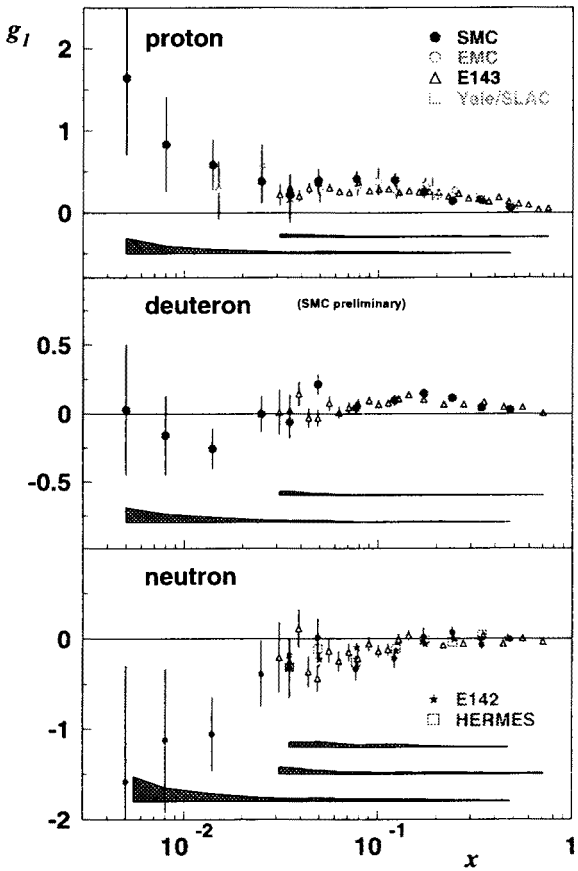

Fig. 6. Structure functions g_1^p, g_1^d and g_1^n at the measured Q^2. Error bars are statistical. The shaded areas show the systematic errors. Figure taken from [45].

and neutron structure functions can be explained by nuclear shadowing in the deuteron, [46].

To evaluate first moments of g_1, a measured $g_1(x, Q^2)$ must be evolved to a scale Q_0^2, common for all x. Previously $g_1(x, Q_0^2)$ was obtained assuming $A_1 \simeq g_1/F_1$ to be independent of Q^2, which is consistent with the data. However QCD predicts the Q^2 dependence of g_1 and F_1 to differ considerably at small x where the experimental acceptance is very limited in Q^2. Therefore the data do not constrain the QCD evolution in the region where large extrapolations in Q^2 are required. Recently calculations of the NLO splitting functions were completed (in the $\overline{MS}$ scheme), [47–49] thus making it possible to perform the NLO QCD evolution of the g_1, [50–52]. The SMC

used the procedure [50] to fit their proton and deuteron data as well as these of EMC and E143. Preliminary results are shown in Fig. 7. Differences between renormalisation schemes and values of strong coupling constants may still change the results considerably.

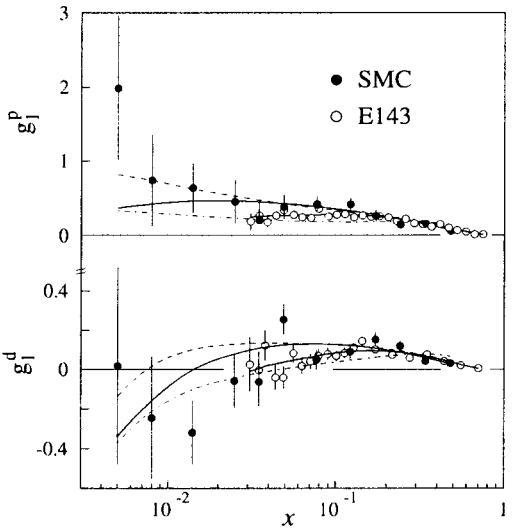

Fig. 7. Results on g_1^p and g_1^d from SMC and E143 at the measured Q^2. Solid curves are NLO QCD fits at Q^2 of data points, dashed — at Q_0^2 =10 GeV^2 and dot-dashed at Q_0^2 =1 GeV^2. Figure comes from [24].

5.2. Tests of the sum rules

Table II shows the collected results for the first moments Γ_1 of g_1 for proton, deuteron and neutron, [45], assuming scaling of A_1. The SMC results for deuteron, [23], and HERMES results, [33], are preliminary. Numbers in parentheses are statistical and systematic errors respectively. The SMC and E143 neutron data result from combining the proton and deuteron results; extrapolating the neutron results to x=0 is a source of major systematic uncertainties, especially for the SLAC data. Results for the SMC proton change by 0.007 if instead of the A_1 scaling assumption, the NLO QCD fit is used to evolve the data to a common value of Q^2. Predicted values of the Ellis–Jaffe sum rules were calculated using the QCD corrections up to the order α_s^3, three quark flavours, $\alpha_s(M_Z^2) = 0.117 \pm 0.005$, $|g_A/g_V|$=1.2573 $\pm$ 0.0028 and F/D=0.575 $\pm$ 0.016. All data consistently violate that sum rules.

TABLE II

Results of the Ellis-Jaffe sum rule measurements. See text for details. Theoretical predictions are given in the bottom section of the table.

Experiment	$\langle Q^2 \rangle$ GeV^2	Proton	Deuteron	Neutron
SMC	10	0.137 (14) (10)	0.038 (7) (5)	-0.055 (24)
E143	3	0.127 (4) (10)	0.042 (3) (4)	-0.037 (8) (11)
E142	2			-0.031 (6) (9)
HERMES	3			-0.032 (13) (17)
Ellis-Jaffe	10	0.170 (5)	0.071 (4)	-0.016 (5)
sum rule	3	0.164 (6)	0.070 (4)	-0.013 (5)
	2			-0.011 (5)

Status of the Bjorken sum rule tests is shown in Fig. 8. Data from all experiments were evolved to $Q^2 \to \infty$ for comparison, using corrections to the order of α_s^3 and constants given above. All the data confirm the sum rule, predicted to give 0.2096 ± 0.0004 at $Q^2 \to \infty$.

Recently a technique of Padé approximants has been suggested for calculating higher order corrections for the flavour nonsinglet sum rules, [55]. As a result, the Bjorken sum depends very strongly on α_s at small Q^2 permitting actually to extract the values of the strong coupling constant: $\alpha_s(M_Z^2) = 0.117^{+0.004}_{-0.007} \pm 0.002$, [55], where the first two errors are statistical and the last one is theoretical.

5.3. Spin structure of the proton

The nucleon spin, $S_z = \frac{1}{2}$, can be decomposed as follows

$$S_z = \tfrac{1}{2}\Delta\Sigma + \Delta g + L_z \tag{16}$$

where L_z is angular momentum due to the partons. Results for Γ_1 shown in Table II, evolved to $Q^2 \to \infty$ using corrections up to α_s^3 together with constants given in the previous section give the following estimate of the flavour singlet axial coupling, $\Delta\Sigma$ and the polarization of the strange sea quarks, Δs. Result is: $\Delta\Sigma \simeq 0.28 \pm 0.07$ and $\Delta s \simeq -0.11 \pm 0.03$ confirming the original EMC conclusion that quark spin contributes little to the proton spin and that the strange sea is indeed polarized opposite to the nucleon spin. The flavor SU(3) breaking (SU(3) was assumed to be exact in the derivation of the above numbers) can decrease Δs but leaves $\Delta\Sigma$ unchanged. Choosing a factorization scheme in which the quarks polarization is scale independent, a Q^2 dependent gluonic contribution appears in the Ellis-Jaffe sum rule

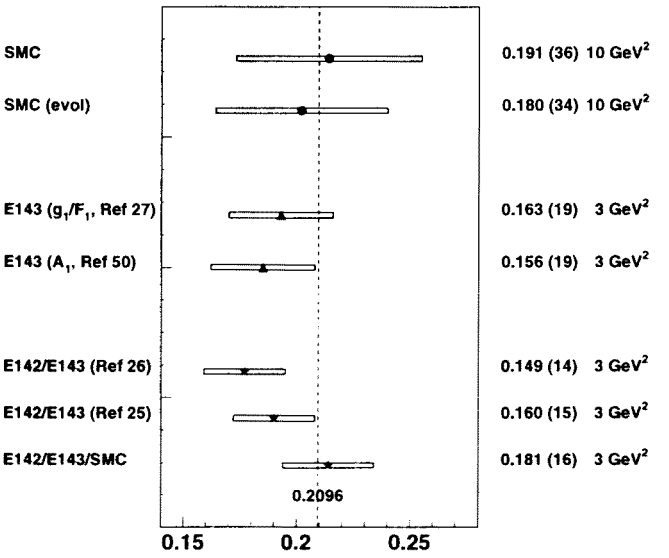

Fig. 8. Results on the Bjorken sum. Data are evolved to $Q^2 \to \infty$ for comparison. The SMC data are preliminary. E143 result assuming that A_1 scales instead of g_1/F_1 was taken from [53]. Figure comes from [54].

as a result of the anomalous dimension of the singlet axial vector current [19]. Then the Ellis-Jaffe assumption of Δs=0 implies that at Q^2=10 GeV^2, $\Delta g \sim 3$ is needed to restore the sum rule. This result is compatible with conclusions from certain QCD analyses, [50].

5.4. Semi-inclusive results

Finally we note the measurements of the semi-inclusive spin asymmetries for positively and negatively charged hadrons in the polarized muon-proton and muon-deuteron scattering in the SMC [56, 45]. Analysing the charged hadrons is the only way of separating quark flavours in the neutral current deep inelastic scattering.

The x dependence of the spin distributions for the up and down valence quarks and for the non-strange sea quarks has been determined. The up valence quarks have positive polarization at all x, while down valence ones are polarized negatively with respect to the proton spin. The moments of the quark spin distributions were obtained to be: Δu_v=0.85±0.0.14±0.12, $\Delta d_v = -0.58 \pm 0.16 \pm 0.11$ and $\Delta \bar{q}$=0.02±0.06±0.03. Here $\Delta \bar{q} = \Delta \bar{u} = \Delta \bar{d}$.

Precise semi-inclusive results are soon expected to come from the HERMES experiment at HERA, *c.f.* [33].

6. Summary and prospects for the future

Understanding of the polarized structure functions has improved dramatically in the recent years, thanks to the EMC, SMC and SLAC measurements. Several questions however remained unanswered. Among them is the low x behaviour of g_1 (somewhat analogous to the unpolarized case), its Q^2 evolution, the gluon polarization and flavour decomposition of polarized parton distribution. The HERMES experiment will especially address the last question from a presently unique reconstruction of the hadronic final state. To answer the remaining questions a new generation of experiments, *e.g.* at the HERA *collider*, is needed. Prospects of spin physics at HERA were discussed at a workshop at DESY–Zeuthen in August 1995, [57]. A polarized deep inelastic programme at HERA could allow measurements over an extended kinematic range, including low x and high Q^2. Polarization of the proton beam is technically much more complicated than polarization of the electron beam, as the proton beam does not polarize naturally. Construction of the polarized proton beams of energy up to 250 GeV in the RHIC collider rings has already been approved, a helpful step for HERA. Unfortunately interpretation of hadron–hadron results from the quark point of view is certainly more complicated. Dedicated measurements of $\Delta g(x, Q^2)$ are however crucial. A precise result can be supplied by the COMPASS project at CERN where 'open charm' production will tag the photon–gluon fusion. Another possibility would be to tag it through measurements of three jets at the HERA collider, *c.f.* [45]. Naturally for the fixed-target data, the non-perturbative effects interfere with the low x dynamics. So there is little doubt that the spin physics will continue to be a field of particular interest.

My thanks to the organizers for the splendid conference and for supporting my attendance and to my colleagues from the NMC and SMC for the enjoyable research collaboration.

REFERENCES

[1] EMC: J. Ashman *et al.*, *Phys. Lett.* **B206**, 364 (1988); *Nucl. Phys.* **B328**, 1 (1989).

[2] H. Abramowicz, plenary talk on the International Conference on High Energy Physics, Warsaw, July 1996.

[3] R.L. Jaffe, *Comments Nucl. Part. Phys.* **19**, 239 (1990).

[4] E.B. Zijlstra, W.L. van Neerven, *Nucl. Phys.* **B417**, 61 (1994); R. Mertig, W.L. van Neerven, Leiden preprint INLO-PUB-6/95 (revised); W. Vogelsang, Rutherford Laboratory preprint RAL-TR-95-071.

[5] T. Gehrmann, W.J. Stirling, Proc. of the Workshop on the Prospects of Spin Physics at HERA, Zeuthen, August 1995, eds. J. Blümlein, W.-D. Nowak, DESY 95-200, p.295.
[6] M.A. Ahmed, G.G. Ross, *Phys. Lett.* **B56**, 385 (1975).
[7] R.D. Ball, S. Forte, G. Ridolfi, *Phys. Lett.* **B378**, 255 (1996).
[8] J. Bartels, B.I. Ermolaev, M.G. Ryskin, *Z. Phys.* **C70**, 273 (1996).
[9] J. Bartels, B.I. Ermolaev, M.G. Ryskin, DESY preprint 96-25 (1996).
[10] R.L. Heimann, *Nucl. Phys.* **B64**, 429 (1973).
[11] S.D. Bass, P.V. Landshoff, *Phys. Lett.* **B336**, 537 (1994).
[12] F.E. Close, R.G. Roberts, *Phys. Lett.* **B316**, 257 (1994).
[13] J.D. Bjorken, *Phys. Rev.* **148**, 1467 (1966); *Phys. Rev.* **D1** (1970) 465; *Phys. Rev.* **D1** (1970) 1376.
[14] S.A. Larin, F.V. Tkachev, J.A.M. Vermaseren, *Phys. Rev. Lett.* **66**, 862 (1991); S.A. Larin, J.A.M. Vermaseren, *Phys. Lett.* **B259**, 345 (1991).
[15] A.L. Kataev, V. Starchenko, *Mod. Phys. Lett.* **A10**, 235 (1995); CERN-TH-7198/94.
[16] J. Ellis, R.L. Jaffe, *Phys. Rev.* **D9**, 1444 (1974); Erratum *Phys. Rev.* **D10**, 1669 (1974).
[17] S.A. Larin, *Phys. Lett.* **B334**, 192 (1994).
[18] A.L. Kataev, *Phys. Rev.* **D50**, 5469 (1994).
[19] C.S. Lam, Bing-An Li, *Phys. Rev.* **D25**, 683 (1982).
[20] R. Voss, Proc. of the Workshop on the Deep Inelastic Scattering and QCD, Paris, April 1995, eds J.-F. Laporte, Y. Sirois, p.77.
[21] SMC: B. Adeva *et al.*, *Phys. Lett.* **B302**, 533 (1993).
[22] SMC: D. Adams *et al.*, *Phys. Lett.* **B357**, 248 (1995).
[23] SMC: D. Adams *et al.*, to be submitted to *Phys. Lett.* **B**.
[24] SMC: D. Adams *et al.*, submitted to *Phys. Rev.* **D**.
[25] SMC: D. Adams *et al.*, *Phys. Lett.* **B329**, 399 (1994); erratum, *Phys. Lett.* **B339**, 332 (1994).
[26] SMC: B. Adeva *et al.*, *Phys. Lett.* **B336**, 332 (1994).
[27] SLAC E142 Collaboration: P.L. Anthony *et al.*, Phys. Rev. Lett. **71**, 959 (1993).
[28] SLAC E142 Collaboration: P.L. Anthony *et al.*, *Phys. Rev.* **B54**, 6620 (1996).
[29] SLAC E143 Collaboration: K. Abe *et al.*, *Phys. Rev. Lett.* **74**, 346 (1995).
[30] SLAC E143 Collaboration: K. Abe *et al.*, *Phys. Rev. Lett.* **75**, 25 (1995).
[31] SLAC E143 Collaboration: K. Abe *et al.*, *Phys. Rev. Lett.* **76**, 587 (1996).
[32] SLAC E154 Collaboration: E. Hughes, presented on the International Conference on High Energy Physics, Warsaw, July 1996.
[33] HERMES Collaboration: W. Wander, presented on the International Conference on High Energy Physics, Warsaw, July 1996.
[34] A. Ogawa (SMC), PhD Thesis, Nagoya University, 1996.

[35] J.M. Le Goff, A. Steinmetz, R. Windmolders, SMC internal note, SMC/96/09.

[36] A. Akhundov *et al., Fortsch. Phys.* **44**, 587 (1996). A.A. Akhundov *et al., Sov. J. Nucl. Phys.* **26**, 660 (1977); **44**, 988 (1986); JINR-Dubna preprints E2-10147 (1976), E2-10205 (1976), E2-86-104 (1986); D. Bardin, N. Shumeiko, *Sov. J .Nucl. Phys.* **29**, 988 (1979).

[37] T.V. Kukhto, N.M. Shumeiko, *Nucl. Phys.* **B219**, 412 (1983).

[38] I.V. Akushevich, N.M. Shumeiko, *J. Phys.* **G20**, 412 (1994).

[39] S. Wandzura, F. Wilczek, *Phys.Lett.* **B72**, 412 (1977).

[40] NMC: P. Amaudruz *et al., Nucl. Phys.* **B371**, 412 (1992).

[41] NMC, P. Amaudruz *et al., Z. Phys.* **C51**, 387 (1991).

[42] EMC: J. Ashman *et al., Z. Phys.* **C57**, 211 (1993).

[43] NMC: M. Arneodo *et al., Phys. Lett.* **B364**, 107 (1995).

[44] L.W. Whitlow *et al., Phys. Lett.* **B250**, 193 (1990).

[45] F. Kunne-Perrot (SMC), presented on the International Conference on High Energy Physics, Warsaw, July 1996.

[46] NMC: M. Arneodo *et al.*, submitted to *Nucl. Phys.* **B**.

[47] E.B. Zijlstra, W.L. van Neerven, *Nucl. Phys.* **B417**, 61 (1994).

[48] R. Mertig, W.L. van Neerven, *Z. Phys.* **C70**, 637 (1996).

[49] W. Vogelsang, *Phys. Rev.* **D54**, 2023 (1996).

[50] R.D. Ball, S. Forte, G. Ridolfi, *Phys. Lett.* **B378**, 255 (1996).

[51] M. Gluck, E. Reya, M. Stratmann, W. Vogelsang, *Phys Rev.* **D53**, 4775 (1996).

[52] T. Gehrmann, W.S. Stirling, *Phys. Rev.* **D53**, 6100 (1996).

[53] J. McCarthy, O.A. Rondon, T.J. Liu, *Phys. Rev.* **D54**, 2391 (1996).

[54] G. Mallot (SMC), Habilitation Thesis, Mainz University, 1996.

[55] J. Ellis *et al., Phys. Lett.* **B366**, 268 (1996); J. Ellis, plenary talk at the SPIN96 conference, Amsterdam, September 1996.

[56] SMC: B. Adeva *et al., Phys. Lett.* **B369**, 93 (1996).

[57] Proc. of the Workshop on the Prospects of Spin Physics at HERA, Zeuthen, August 1995, eds J. Blümlein and W.-D. Nowak, DESY 95-200, p.76-99.